Inter-machine validation study of neoclassical transport modelling in medium- to high-density stellarator-heliotron plasmas

2013 Nucl. Fusion 53 063022

(http://iopscience.iop.org/0029-5515/53/6/063022)

Nucl. Fusion **53** (2013) 063022 (8pp) doi:10.1088/0029-5515/53/6/063022

Inter-machine validation study of neoclassical transport modelling in medium- to high-density stellarator-heliotron plasmas

A. Dinklage[1], M. Yokoyama[2], K. Tanaka[2], J.L. Velasco[3], D. López-Bruna[3], C.D. Beidler[1], S. Satake[2], E. Ascasíbar[3], J. Arévalo[3], J. Baldzuhn[1], Y. Feng[1], D. Gates[4], J. Geiger[1], K. Ida[2], M. Isaev[5], M. Jakubowski[1], A. López-Fraguas[3], H. Maaßberg[1], J. Miyazawa[2], T. Morisaki[2], S. Murakami[6], N. Pablant[4], S. Kobayashi[2], R. Seki[2], C. Suzuki[2], Y. Suzuki[2], Yu. Turkin[1], A. Wakasa[6], R. Wolf[1], H. Yamada[2], M. Yoshinuma[2], LHD Exp. Group[2], TJ-II Team[3] and W7-AS Team[1]

[1] Max-Planck-Institut für Plasmaphysik, EURATOM Association, Greifswald, Germany
[2] National Institute for Fusion Science, Toki, Japan
[3] The National Fusion Laboratory, CIEMAT, EURATOM Association, Madrid, Spain
[4] Princeton Plasma Physics Laboratory, Princeton, NJ, USA
[5] National Research Center 'Kurchatov Institute', Moscow, Russia
[6] Department of Nuclear Engineering, Kyoto University, Kyoto, Japan

E-mail: dinklage@ipp.mpg.de

Received 21 December 2012, accepted for publication 23 April 2013
Published 17 May 2013
Online at stacks.iop.org/NF/53/063022

Abstract
A comparative study of energy transport for medium- to high-density discharges in the stellarator-heliotrons TJ-II, W7-AS and LHD is carried out. The specific discharge parameters are chosen to apply a recently concluded benchmarking study of neoclassical (NC) transport coefficients (Beidler *et al* 2011 *Nucl. Fusion* **51** 076001) to perform this validation study. In contrast to previous experiments at low densities for which electron transport was predominant (Yokoyama *et al* 2007 *Nucl. Fusion* **47** 1213), the current discharges also exhibit significant ion energy transport. As it affects the energy transport in 3D devices, the ambipolar radial electric field is addressed as well. For the discharges described, *ion-root* conditions, i.e. a small negative radial electric field were found. The energy transport in the peripheral region cannot be explained by NC theory. Within a 'core region' ($r/a < 1/2 \sim 2/3$), the predicted NC energy fluxes comply with experimental findings for W7-AS. For TJ-II, compliance in the core region is found for the particle transport and the electron energy transport. For the specific LHD discharges, the core energy transport complied with NC theory except for the electron energy transport in the inward-shifted magnetic configuration. The NC radial electric field tends to agree with experimental results for all devices but is measured to be more negative in the core of both LHD and TJ-II. As a general observation, the energy confinement time approaches the gyro-Bohm-type confinement scaling ISS04 (Yamada *et al* 2005 *Nucl. Fusion* **45** 1684). This work is carried out within the International Stellarator-Heliotron Profile Database (www.ipp.mpg.de/ISS and http://ishpdb.nifs.ac.jp/index.html).

(Some figures may appear in colour only in the online journal)

1. Introduction

Stellarator-heliotrons (S-H) offer an alternative route to steady-state fusion reactors. One central mission of the largest S-H devices is to provide a physics basis for burning S-H plasmas. Consequently, the S-H devices closest to reactor conditions play key roles: the Large Helical Device (LHD, in operation) and Wendelstein 7-X (W7-X, under construction). In contrast to tokamaks, 3D magnetic fields in S-H lead to localized, trapped particles even in the plasma core. These

particles significantly enhance the radial neoclassical (NC) transport particularly for reactor-relevant conditions, i.e. when the plasma is sufficiently hot and both the electrons and ions are in the long-mean-free-path (lmfp) regime. At the same time, the discharges have a relatively high plasma density to simulate the most efficient reactor conditions for which thermal equilibration ($T_e \approx T_i$) can be expected.

In 3D magnetic configurations, a radial electric field (E_r) must arise to comply with the ambipolarity condition, which is not intrinsically satisfied as in axisymmetric tokamaks. The resulting E_r primarily affects the transport coefficient for the ions (placing the ions in the so-called $\sqrt{\nu}$-regime, see [1] and references therein). In the lmfp at sufficiently high densities, E_r is anticipated to satisfy the so-called ion-root solution for ambipolar particle fluxes, i.e. a relatively small, negative radial electric field. Moreover, even assuming electrostatic turbulence (which in leading order is intrinsically ambipolar) for the peripheral region, the NC ambipolar particle fluxes can be expected to determine E_r. Summarizing, the comparison of E_r and the energy fluxes from NC theory with experimentally determined fluxes from the heating sources and energy sinks is a cornerstone for a conclusive validation of NC theory.

A recently concluded benchmarking of calculations of transport coefficients from local NC theory [1] allows now a quantitative experimental energy transport study. While in earlier inter-machine studies of NC transport in 3D devices the electron energy transport at low densities has been investigated [2], this study focuses on the energy transport at medium- to higher densities as anticipated when approaching reactor conditions. At these densities $n_e > 4 \times 10^{19}\,\mathrm{m}^{-3}$, also the ion energy transport significantly affects the energy confinement. Since NC transport in 3D devices shows most unfavorable temperature scalings, NC transport becomes increasingly predominant as the temperature is increased and the purpose of this study is the validation of local NC theory at these reactor-relevant conditions. Nevertheless, LHD discharges in previous documentations have revealed that the NC contribution accounts for only a part of experimentally evaluated energy flux [4–7] indicating that the specific plasma conditions and magnetic configurations may lead to different transport channels. The strategy for this assessment, however, was to choose plasma conditions for which clear NC predictions exist and for which other transport channels are expected to be less important. This approach led to the specific choices of discharges in W7-AS and to dedicated experiments in TJ-II and LHD. Based on this study, further exploration of predicted dependences will be performed in follow-up studies.

Consequently, the experimental conditions for this study are chosen to focus on NC transport. Although the NC ion transport coefficients are expected to exceed the electron ones for the envisaged conditions, typical temperatures for which the NC electron energy diffusivity exceeds a value of $\chi_e^{NC} > 1\,\mathrm{m}^2\,\mathrm{s}^{-1}$ can be estimated as a figure for applicability of NC theory. At half of the minor plasma radius, those temperatures lie in the range from about 400 eV (TJ-II) to 1.3 keV (W7-AS) to 1.8–2.4 keV (LHD) at densities of $n = 4 \times 10^{19}\,\mathrm{m}^{-3}$. Aiming at these rough density and temperatures, discharges are assessed with regard to NC transport predictions for three major S-H devices: TJ-II [8], Wendelstein 7-AS [9] and LHD [10].

Table 1. Survey of parameters relevant to this study.

	TJ-II	W7-AS	LHD STD	LHD IWD
R_0 (m)	1.5	2	3.75	3.60
a (m)	0.19, 0.17	0.17	0.60	0.62
B_0 (T)	0.95	2.52	2.64	2.75
$\iota_{2/3}$	1.46, 1.55	0.34	0.83	0.86
N	4	5	10	
P_{abs} (MW)	0.6, 0.34	1.9, 1.4, 0.4	16.2	15.9
T_i^0 (keV)	0.14	0.7, 1.2, 1.1	1.1	1.8
n_0 ($10^{19}\,\mathrm{m}^{-3}$)	6	11.3, 6.3, 11.0	4.1	4.2
τ_E^{exp} (ms)	2.6, 3.4	8, 13, 32	37	73

Note: R_0: major radius, a: minor radius, B_0: magnetic field on axis, $\iota_{2/3}$: rotational transform at 2/3 of the minor plasma radius, N: number of toroidal periods, P_{abs}: absorbed heating power, T_i^0: central ion temperature, n_0: central electron density, τ_E^{exp}: experimentally determined energy confinement time.

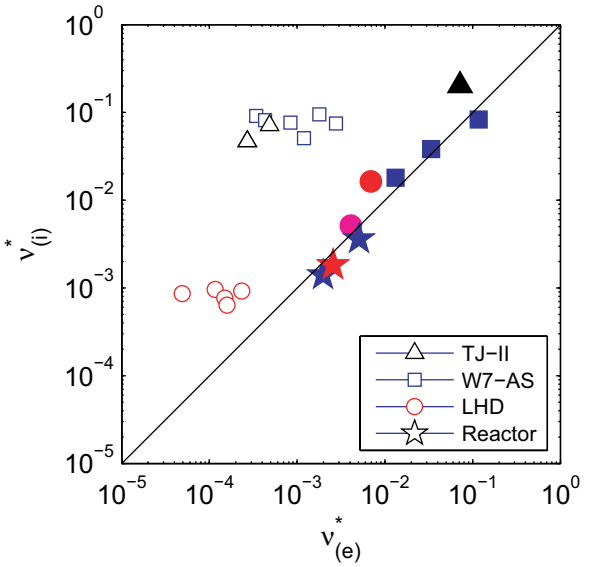

Figure 1. Central electron ($\nu_e^\star$) and ion collisionality ($\nu_i^\star$) at the respective thermal velocity $v_{th} = (k_B T/m)^{1/2}$ for ISHPDB datasets for NC theory assessments. The full symbols represent the discharges in this study. The open symbols correspond to CERC discharges [2], the stars are reactor scenarios (red star: 4× LHD [23], blue star: HELIAS ignition scenarios [24]). The shapes of the symbols correspond to the devices TJ-II, W7-AS and LHD as indicated.

2. Experimental approach

Table 1 summarizes the data sets and device parameters of this study. For LHD, two cases with differing magnetic configurations are assessed: the *standard configuration* with a major axis of $R_0 = 3.75$ m (STD) and the *inward-shifted configuration* ($R_0 = 3.6$ m) (IWD). Figure 1 shows the central electron and ion collisionality ($\nu_{e,i}^\star = R_0 \nu/(v_{e,i}^{th} \iota)$, R_0: major radius, ν: 90° collision frequency, $v_{e,i}^{th}$: thermal velocity of electrons and ions, respectively, ι: rotational transform) along with reactor-relevant values indicating thermal equilibration $\nu_e^\star \approx \nu_i^\star$ is attained. In addition to the datasets analysed in this paper, figure 1 shows collisionalities attained in previous studies of NC transport at lower densities with strong electron heating. This led to lower electron collisionalities and the establishment of the *core electron root confinement* (CERC) regime characterized by higher central electron temperatures

and positive radial electric fields affecting the transport in the plasma core [2]. In contrast, in this study, equilibrated reactor ion collisionalities are increasingly approached in the sequence from TJ-II → W7-AS → LHD STD → LHD IWD. The higher central ion temperatures due to a more and more intense ion heating lead to higher ion temperature gradients. Thus the ion energy transport becomes increasingly relevant in contrast to the CERC discharges. A specific quantification of the energy transport in the ion channel with regard to the electron heat transport, however, requires in addition the consideration of the radial electric field (and its impact on the transport coefficients) and the density gradients to form the full transport matrix.

The specific NC transport coefficients were calculated by convoluting the local monoenergetic transport coefficients as described in [1]. As a general guide-line for the experimental documentation, profile measurements of electron and ion temperatures, the electron density, E_r profiles, estimates for Z_{eff}, waveforms indicating stationary discharge conditions and equilibria are collected. For the experimental conditions addressed in this paper, the determination of both the electron and ion temperatures is crucial to properly account for the energy transfer between electrons and ions ($P_{\mathrm{ei}} \propto n_{\mathrm{e}}^2(T_{\mathrm{e}} - T_{\mathrm{i}})/T_{\mathrm{e}}^{1.5}$). It should be noted that this requirement for a full experimental documentation represents a technical problem for validation studies as done in this paper: it is a prerequisite to collect full sets of local measurements to determine the thermodynamic forces along with the magnetic configurations, energy and particle sources and sinks and so on. Consequently, the validation of specific theories requires dedicated experiments with a high level of diagnostics input.

The validation approach as done here is to compare two fluxes: first, the 'NC flux' is determined with the NC transport coefficients [1] and the gradients of the experimental density and temperature profiles. Second, the sources from deposition calculations considering heating and particle sources (the latter where available) yield the 'experimental flux'. Both fluxes are compared and the NC radial electric field E_r^{NC} is compared with measurements of E_r where available.

Technically, the steady-state energy balance analyses were performed using the integrated transport code TASK3D [11] for LHD discharges. In TJ-II, the studied plasmas are non-stationary and the balance analysis is carried out following the time evolution with the ASTRA [12] package. For W7-AS, the experimentally determined particle and energy fluxes were compared with NC fluxes with transport coefficients from DKES. The following paragraphs summarize the experimental results for TJ-II, W7-AS and LHD.

2.1. TJ-II

The plasma parameters in TJ-II discharges were obtained with the following diagnostics: Thomson scattering (electron density n_{e} and temperature T_{e}); edge He-beams (n_{e} and T_{e} in $0.7 \lesssim r/a \leqslant 1$ with r being the flux-surface label and a the plasma minor radius); interferometry (line density); reflectometry (n_{e} in $0.7 \lesssim r/a \leqslant 1$); charge-exchange neutral particle analyser (CX-NPA) for core ion temperature and CX fluxes; several bolometer arrays for radiation and heavy-ion beam probe (HIBP) for plasma potential measurements. The ion temperature profile is assumed to be proportional

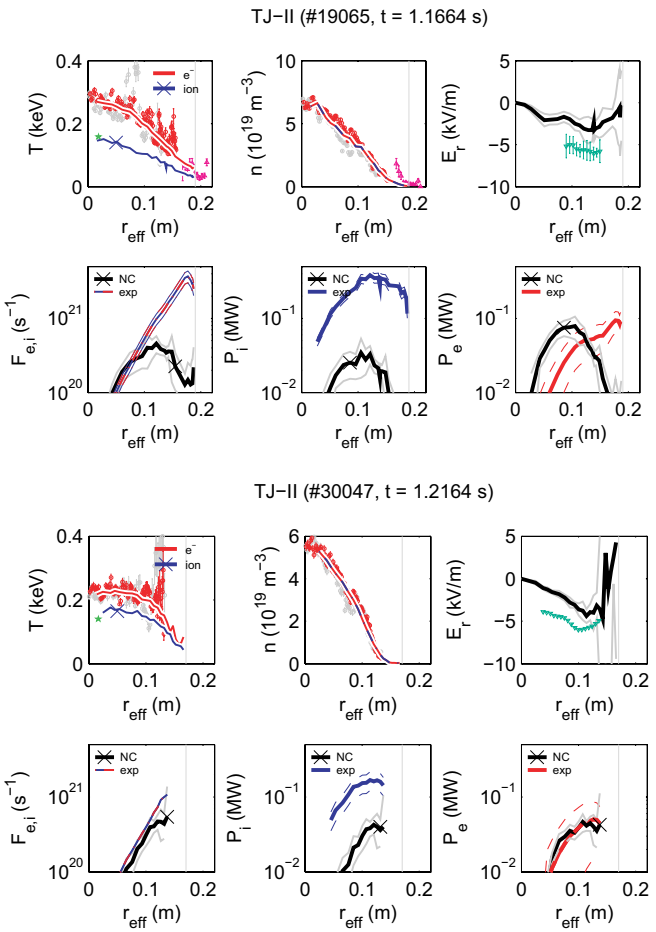

Figure 2. Transport analysis for the TJ-II discharges #19065 and #30047. T_{e} and n_{e} come from Thomson scattering (red) and helium beam measurements (magenta), the T_{i}-profiles are proportional to the n_{e}-profile adjusted to central CXRS-NPA data (green star). E_r data are results from heavy-ion beam probe measurements (green triangles). $F_{\mathrm{e,i}}$ are the total electron and ion particle fluxes, respectively. $P_{\mathrm{e,i}}$ are the total energy fluxes. NC predictions are plotted as black lines with error margins. The grey vertical lines indicate the position of the last closed flux surface. The markers attached to lines (crosses) are to indicate lines in a black/white copy.

to the density profile and centrally adjusted to the CX-NPA measurements [17]. For the mapping on flux surface, vacuum configurations were used (low-β). Since the presence of magnetic resonances can alter transport significantly, a magnetic configuration that excludes them is chosen for the analysis. Joint fits of the experimental profiles are performed within an *integrated data analysis* [13]. For the experimental fluxes, the recycling particle sources (no gas puffing) and NBI deposition are considered.

Figure 2 shows power balances for the discharges #19065 and #30047. Discharge #19065 has been discussed in [14]. Discharge #30047 corresponds to a configuration of smaller effective helical ripple for which non-local effects are expected to be smaller. Nevertheless, no qualitative difference is observed among the two discharges. The measured electric field is systematically stronger than the NC prediction. Reflectometry and passive spectroscopy data for similar discharges measure radial electric fields compatible with the HIBP measurements shown here. This discrepancy has been attributed earlier to non-local NC effects, which is a correction in the NC flux and ambipolar-E_r calculations by

taking account of finite radial excursions of guiding-centre orbits [15, 16].

The predicted particle and electron energy fluxes agree with the experimental estimates within 2/3 of the plasma radius for #30047, the ion energy flux from experimental sources is about one order of magnitude larger over all radii. For discharge #19065, the compliance for the particle fluxes is restricted to 1/2 of the minor radius, the electron energy fluxes are too low in the core but exceed the NC predictions for $r/a > 2/3$. The ion energy flux does not comply for all plasma radii as for #30047. The plasma complies with ion-root conditions [17]: a negative electric field is formed to reduce the ion transport to the electron level but the absolute value is more negative in the experiments and hardly compatible with the uncertainties of NC calculations and experimental errors.

2.2. W7-AS

Figure 3 shows results for the assessed W7-AS discharges. The ion temperature profile data were determined from neutral particle analysis (NPA) and charge-exchange recombination spectroscopy (CXRS). The electron temperature profiles were determined by Thomson scattering and electron cyclotron emission radiometry. The measurements of the radial electric field are from CXRS poloidal rotation measurements and line-integrated spectroscopy on BIV. There were no E_r measurements for shot #34187. The mapping to effective radii employs equilibrium calculations. The resulting symmetrized kinetic profiles were fitted with smooth fit functions which are the basis for the calculation of the temperature and density gradients. The experimental particle fluxes were determined by neutral gas modelling fitting with calibrated H_α emission signals to determine the recycling neutral fluxes from the wall and from gas puffing. The particle and power deposition by neutral beam injection were determined with deposition calculations. Full power deposition by electron cyclotron heating was included where applicable. The discharges #34313 and #34609 have been described in [18] in more detail.

The documentation of shot #34187 is lacking both E_r measurements and the particle sources. We included the shot as an example for very high confinement time and with dominating ion transport. The comparison of E_r indicates for the shots #34313 and #34609 agreement of the measurements and the E_r from the ambipolarity condition virtually for the entire confined plasma. There are discrepancies, however, close to the last closed flux surface which are not understood. Local NC theory appears to be not applicable for the fields observed but experimental results are also contradictory. The particle fluxes for the shots #34313 and #34609 are in excellent agreement within 2/3 of the last closed flux surface. The same applies for the energy flux of both the ions and the electrons. For #34187 agreement of the NC ion energy flux is found with experimental results, however, the NC electron energy flux disagrees significantly. But for this case, $T_e - T_i$ appears to be quite inaccurate and the sum of the 'NC' ion and electron fluxes agrees well with the 'experimental' fluxes.

In the plasma core, NC theory complies with the experimental findings. At outer plasma radii ($r_{eff}/a > 0.7$) at lower temperatures, NC theory increasingly underestimates both the particle and the energy fluxes. The region of discrepancy also coincides with some differences of the E_r measurements with the NC ambipolarity condition. The core region complies with ion-root conditions.

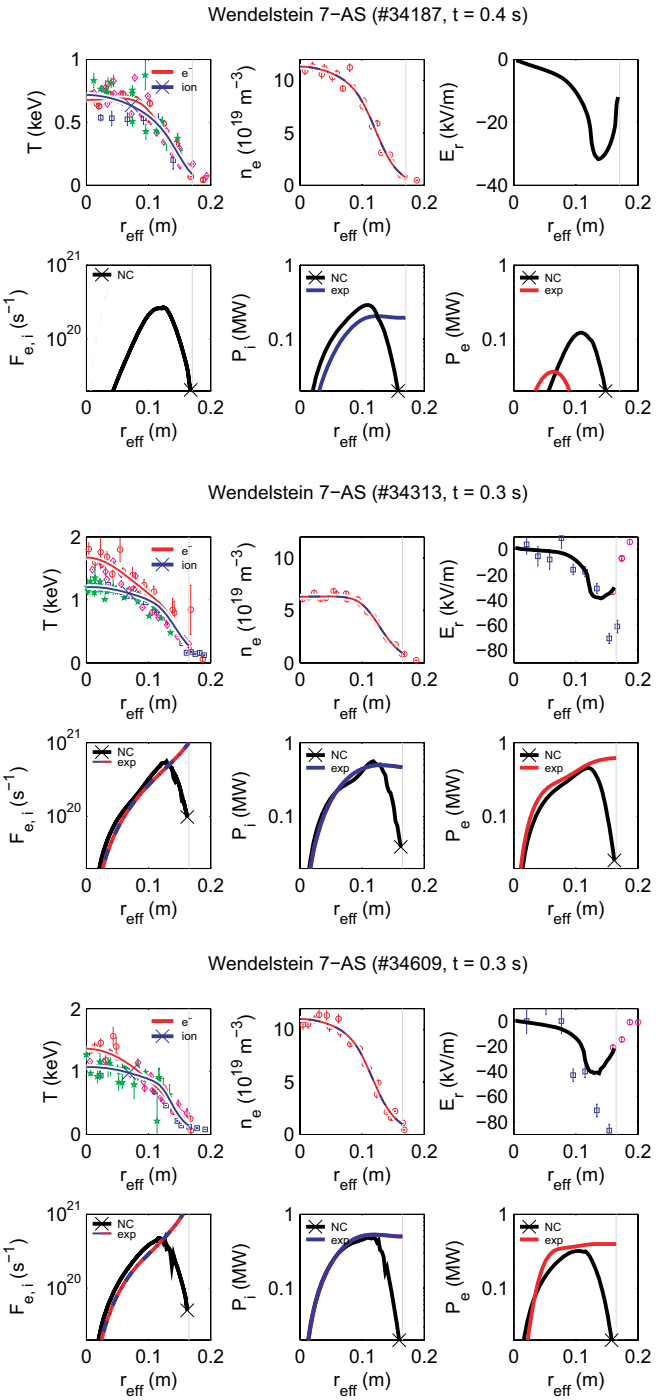

Figure 3. Transport analysis W7-AS (for #34313 and #34609 see [18]). Open red circles are Thomson scattering data (n_e, T_e). Magenta diamonds are ECE measurements (T_e), blue squares are from CXRS (T_i, E_r), green stars from NPA (T_i) and magenta circles from passive BIV spectroscopy (E_r). The grey vertical lines indicate the position of the last closed flux surface. The markers attached to lines (crosses) are to indicate lines in a black/white copy.

2.3. LHD

Figure 4 shows results for two LHD discharges at the highest available heating power. The difference of discharge #109696 (IWD) and #109718 (STD) is mainly the magnetic

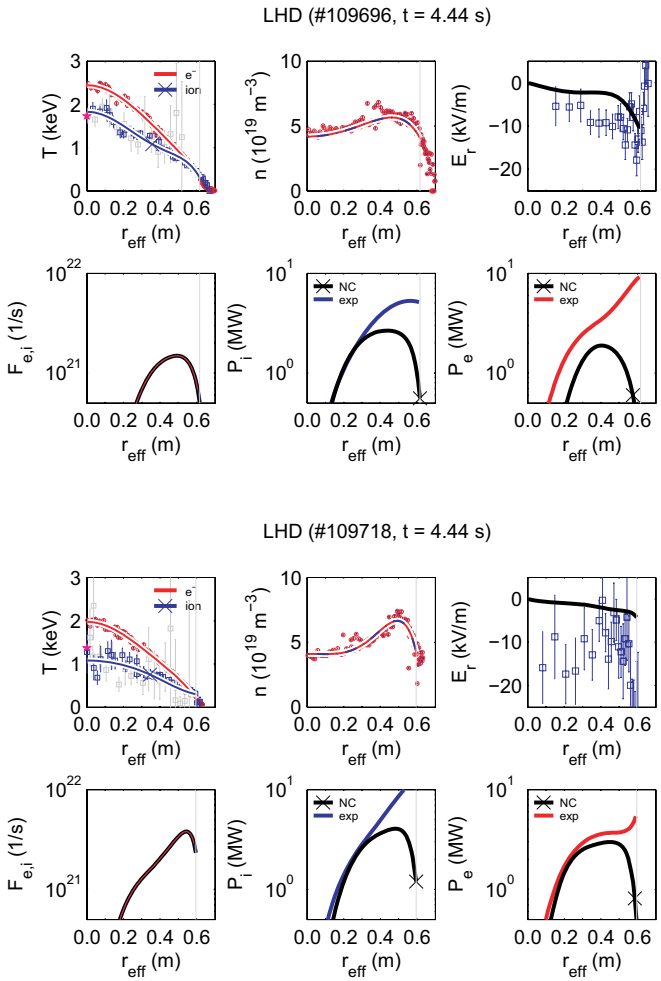

Figure 4. Transport analysis for LHD discharges (#109696 and #109718). T_e and n_e come from Thomson scattering, T_i from CXRS (grey T_i data from inboard-side measurements) and a central value from x-ray imaging (magenta star). E_r data are $\delta t \pm 15$ ms weighted-averaged CXRS measurements. The markers attached to lines (crosses) are to indicate lines in a black/white copy.

configuration. Due to the inward shift of the plasma, the magnetic configuration shows improved NC confinement (σ optimization, see [19] for more details). Addressing the validity of NC theory, the comparison of different NC transport properties within a single device is of particular interest for this study.

The ion temperature profile data were determined from CXRS and a measurement of a newly installed x-ray imaging spectroscopy is added to confirm the CXRS data. The electron temperature profiles are determined by Thomson scattering. The measurement of the radial electric field is from CXRS polodial rotation measurements. The experimental data were mapped from real space coordinates to effective radii using mapping routines based on a database of equilibrium calculations [20]. The resulting profiles are fitted with smooth fit functions which are the basis for the calculation of the temperature and density gradients. The particle and power deposition by neutral beam injection are determined with deposition calculations [21].

The measurement of the radial electric field tends to agree for #109696 but appears to be systematically more negative than the predicted ambipolar radial electric field. The CXRS E_r measurements suffer from beam attenuation effects due to high densities. Due to the resulting small signal-to-noise ratio, the measurements are weighted averaged (± 15 ms) over a period considerably smaller than variation times of the plasma parameters. For #109718 there are large discrepancies in the core between measurements and predictions of the ambipolar field. Experimentally, again high densities may affect the E_r measurement. The relevance of non-local effects [15, 16, 22] needs further assessments.

The energy fluxes are mainly found to be in agreement with the NC prediction obtained with the DGN/LHD transport package [26] in the plasma core. The region of agreement appears to be somewhat larger for the STD configuration than for the inward-shifted configuration. The NC electron heat transport in the inward-shifted case, however, is significantly lower than the results from the analysis with the DGN/LHD transport package. Since the experimental kinetic energy content is found to be smaller than the diamagnetic energy, a systematic sensitivity study was carried out to quantify the effect of a $\pm 10\%$-β variation. The result is a $+30\%/-15\%$ variation in the electron energy flux and somewhat lower for the ions. A more thorough assessment of the impact of NBI slowing down particles on W_{dia} is to be addressed in forthcoming studies. The assessed cases comply with ion-root conditions. It is also noted that the NC ion energy flux sensitively depends on the specific value of the radial electric field and decreases with a more negative radial electric field in the $\sqrt{\nu}$ transport regime. All discharges show a hollow density profile which stays constant or varies on time scales larger than the energy confinement time. The hollowness apparently indicates thermodiffusion compensating the inward directed particle flux driven by the positive density gradient in the core plasma. Experimental data for the particle sources are lacking and the particle balance will be addressed in forthcoming studies extending existing analyses of the particle transport [29] to collisionalities as addressed in this study.

3. Core energy transport and the impact on energy confinement

In order to discuss the transport mechanism in the assessed medium- to high-density, lmfp discharges, figure 5 shows more details of the NC power balance for the previously discussed LHD discharge #109696. The plasma is heated in its volume by NBI with no specific peaking of the heating sources. The ratio of electron to ion heating is affected by the proportion of fast negative NBI with dominant electron heating and slower positive NBI with more ion heating. The NBI also fuels the discharges from the peripheral region up to the centre. Particle sources at the edge are due to recycling fluxes and gas puffing.

The resulting ion and electron temperature profiles are peaked in the centre and the density profiles are hollow with a flat region in the centre and a density maximum in the peripheral region at about the maximum penetration depth of the recycling fluxes ($r_{\mathrm{eff}}/a \approx 0.8$). A detailed discussion of particle transport, however, is not addressed in this paper. The particle transport in LHD has been discussed in [29].

Figure 5(a) indicates that the main outward pointing thermodynamic forces are the electron and ion temperature gradients ($L_T^{-1} = |\nabla T|/T$). The negative ambipolar radial

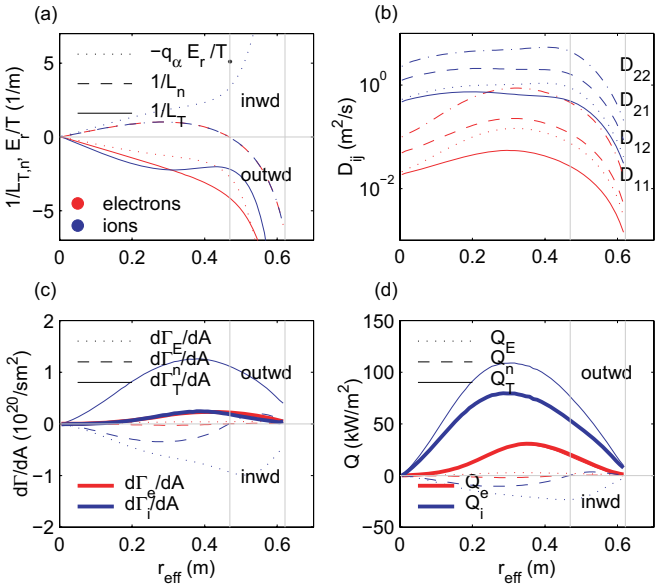

Figure 5. Power balance for LHD discharge #109696 (see also figure 4) and associated figures (thermodynamic forces, transport coefficients, NC particle flux densities, NC energy flux densities). The grey lines indicate the position of the flux surface enclosing 99% of the plasma energy and the off-axis maximum of the density profile, respectively.

electric field (E_r) drags the ions inward ($q_\alpha = Ze$) and pushes the electrons outwards ($q_\alpha = -e$). An inward directed force is due to the positive density gradient L_n^{-1} where the density profile is hollow. It is noted that this is different to the peaked or flat density profiles as shown from TJ-II and W7-AS.

With these contributions to the thermodynamic forces, the particle fluxes and the energy fluxes can be calculated by

$$\Gamma_\alpha = -n_\alpha \left[D_{11}^\alpha \left(L_{n_\alpha}^{-1} - \frac{q_\alpha E_r}{T_\alpha} \right) + D_{12}^\alpha L_{T_\alpha}^{-1} \right], \qquad (1)$$

$$\frac{Q_\alpha}{T_\alpha} = -n_\alpha \left[D_{21}^\alpha \left(L_{n_\alpha}^{-1} - \frac{q_\alpha E_r}{T_\alpha} \right) + D_{22}^\alpha L_{T_\alpha}^{-1} \right]. \qquad (2)$$

Figure 5(b) shows the calculated radial dependences of the transport coefficients as determined from the local monoenergetic transport coefficients (see [1]) also taking into account E_r: D_{22} and D_{21} for the energy fluxes due to L_T^{-1} and L_n^{-1}; D_{12} and D_{11} for the particle fluxes, respectively. The ion transport coefficients are much larger than the electron transport coefficients. The transport coefficients of the ions depend much more on the radial electric field than those of the electrons and get smaller when E_r gets more negative.

Figures 5(c) and (d) reflect the contributions of the thermodynamic forces (see figure 5(a)) to the NC local particle and energy flux densities, respectively. For the electrons, the total fluxes are mainly driven by the electron temperature gradient (the corresponding thin line is covered by the bold line of total flux densities in figures 5(c) and (d)). The contributions due to the density gradient and the radial electric field are small compared with the temperature-gradient-driven fluxes for the electrons. For the ions, in contrast, the inward directed particle flux density (figure 5(c)) due to the radial electric field and the density-gradient-driven flux in the core region needs to be overcompensated by thermodiffusion to fulfil the ambipolarity

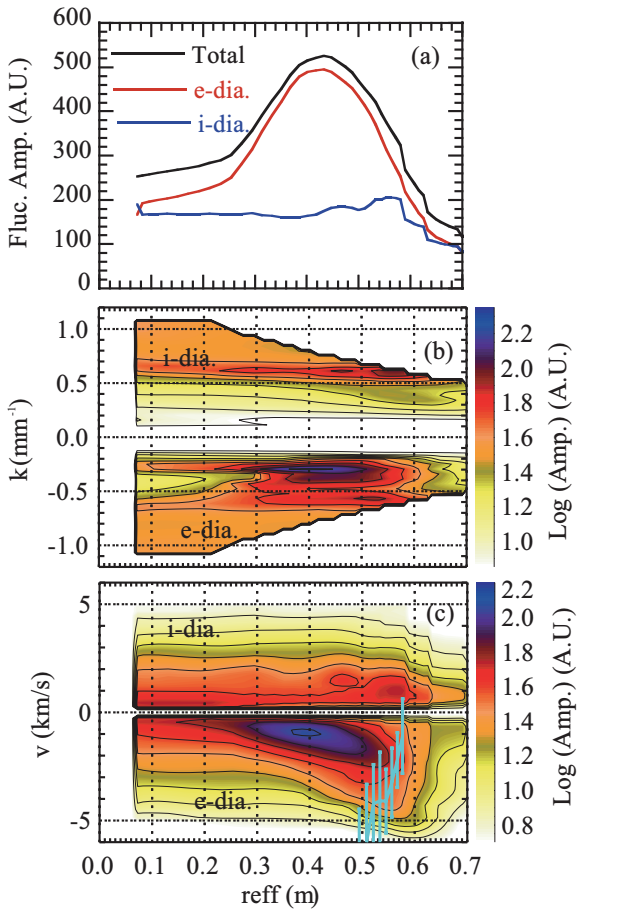

Figure 6. Results of fluctuation measurements for LHD discharge #109696. k is the wavenumber of the fluctuations and v the velocity of fluctuations. e-dia and i-dia refer to the electron- and ion-diamagnetic direction, respectively.

condition $\Gamma_e = Z\Gamma_i$. For the ion energy flux densities, the temperature-gradient-driven term is partially compensated by the inward directed density gradient and radial electric field terms.

In this picture of local NC transport, the ion transport coefficient is adjusted to an E_r satisfying $\Gamma_e = Z\Gamma_i$. For the hollow density profile discussed here, a smaller $|E_r|$ is required due to the positive density gradient. This, in turn, is reflected by the much larger ion transport coefficients in figure 5(b).

Figure 6 shows fluctuation measurements by a phase-contrast imaging method [25]. The measurements indicate large fluctuation amplitudes in the peripheral region which corresponds to the outer radii for which the experimentally determined energy fluxes begin to deviate considerably from the NC energy fluxes (see figure 4). The wave numbers of about 0.1–0.4 mm^{-1} found with the phase-contrast turbulence measurements are compliant with TEM or ITG type turbulence. These findings suggest that the assessed discharges consist of a core being compliant with the NC predictions and a periphery which cannot be described by NC theory.

In order to discuss the result with regard to overall performance figures, figure 7 shows the energy confinement time of the discharges assessed in this study in comparison with a multi-machine scaling law ISS04 [3]. It is found that the overall performance resembles quite well the 0D scaling ISS04. Some configuration effects like an enhanced

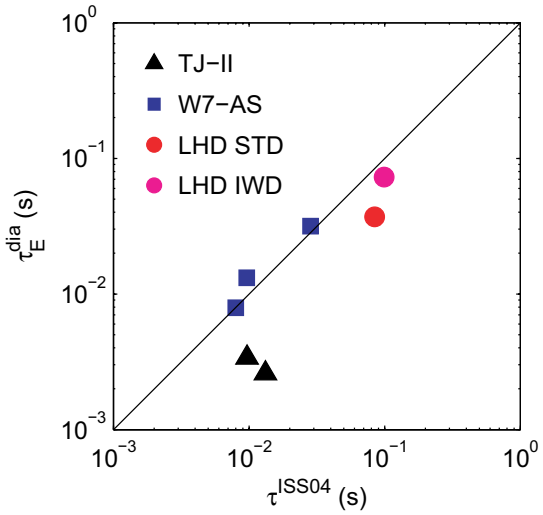

Figure 7. Confinement time of the assessed discharges versus ISS04 prediction [3].

confinement in the inward-shifted case compared with the standard configuration of LHD and a renormalization factor of about 0.4 for TJ-II are in line with the assessment of the much larger stellarator-heliotron confinement database [27]. A conclusion supported with figure 7 is that—although exhibiting NC transport in the core—the confinement is still compliant with a gyro-Bohm scaling for the energy confinement. For upscaling an existent device to reactor size, it will be necessary to understand in more detail the formation of the peripheral region and how the size of a NC core scales with increasing plasma volume.

4. Discussion and summary

Summarizing, an inter-machine dataset covering devices of different size and a variety of magnetic configurations is comprehensively analysed to assess the ranges of validity of NC transport predictions in medium- to high-density, high temperature discharges. In TJ-II the NC particle fluxes and electron energy fluxes agree within $r/a < 1/2 \sim 2/3$. The NC prediction for the ion energy flux does not match at all. The radial electric field is found to reflect ion-root conditions but differs from measurements significantly ($|E_r^{NC}| < |E_r^{exp}|$). For the assessed W7-AS plasmas, NC theory is consistent with experimental findings for Γ and $Q_{e,i}$ within $r/a < 2/3$. There are some differences in E_r for the outermost radii. In the selected LHD discharges, large contributions of NC ion transport to the overall energy fluxes are found both in the standard and the inward-shifted magnetic configuration for $r/a < 0.7$. The electron energy flux complies with NC predictions for the STD case in the same region but appears to be underpredicted for the IWD configuration even in the core region. The radial electric field measured by CXRS shows differences to the ambipolar E_r specifically for the STD case in the plasma core.

For all discharges (TJ-II, W7-AS, LHD), transport in the peripheral region cannot be explained by NC theory. For LHD, this region coincides with increasing fluctuations at normalized wavenumbers possibly indicating turbulent transport mechanisms of TEM or ITG type. The radial electric fields reflect ion-root conditions, but experimental values of E_r are systematically more negative in TJ-II and LHD.

This study gives rise to follow-up investigations to address non-local effects such as finite radial width of trapped particle orbits and direct particle loss near the last closed flux surface and the validity of the monoenergetic approximation used in standard local NC calculations [1] needs to be investigated.

For densities $n > 4 \times 10^{19}\,\mathrm{m}^{-3}$ and temperatures above some keV, it can be concluded that the NC energy fluxes significantly contribute to or even fully comply with experimental findings. Nevertheless, larger discrepancies to NC predictions are found in adjacent parameter regimes in LHD (e.g. [28]). The global confinement for the assessed parameter range complies well with the ISS04 energy confinement scaling for the larger devices.

As an outlook and also pointed out by the hollow density profiles observed in LHD [29], it is emphasized that the coupling of NC energy and particle transport is highly relevant for the discharge scenario development for large S-H devices and reactor operation scenarios. This issue therefore requires further documentation and deeper understanding, e.g. in view of density control [30] or impurity transport in 3D devices. With regard to the strategy for attaining a comprehensive physics basis for S-H reactors, this study pursues the creation of a more extended inter-machine database of reactor-relevant parameter regimes. An open issue is the inter-machine comparison for discharge parameters expected to show different transport mechanisms.

Acknowledgments

The authors would like to thank the LHD experiment group and the technical staff of LHD, the TJ-II Team (with special thanks to the HIBP group) and the W7-AS Team for their support of this work. The joint experiment conducted in LHD was supported by National Institute for Fusion Science (NIFS)/National Institutes of Natural Sciences (NINS) under the project, 'Promotion of the International Collaborative Research Network Formation' (NIFSKEIN1107). This work is also partly supported under the auspices of the NIFS Collaboration Research program (NIFSKNTT008 and NIFSKLPT001).

References

[1] Beidler C.D. *et al* 2011 *Nucl. Fusion* **51** 076001
[2] Yokoyama M. *et al* 2007 *Nucl. Fusion* **47** 1213
[3] Yamada H. *et al* 2005 *Nucl. Fusion* **45** 1684
[4] Ida K. *et al* 2003 *Phys. Rev. Lett.* **91** 085003
[5] Murakami S. *et al* 2007 *Fusion Sci. Technol.* **51** 112
[6] Yamada H. *et al* 2008 *Plasma Fusion Res.* **3** S1032
[7] Nagaoka K. *et al* 2011 *Nucl. Fusion* **51** 083022
[8] Sanchez J. *et al* 2011 *Nucl. Fusion* **51** 094022
[9] Hirsch M. *et al* 2008 *Plasma Phys. Control. Fusion* **50** 053001
[10] Komori A. *et al* 2010 *Fusion Sci. Technol.* **58** 1
[11] Yokoyama M. *et al* 2012 *Plasma Fusion Res.* **7** 2403011
[12] Pereverzev G.V. 2002 ASTRA—An automatic system for transport analysis in tokamaks *IPP Report* 5/98, Max-Planck-Institut für Plasmaphysik, Garching
[13] Van Milligen B. *et al* 2011 *Rev. Sci. Instrum.* **82** 073503

[14] Lopez-Bruna D. *et al* 2013 *Plasma Phys. Control. Fusion* **55** 015001
[15] Tribaldos V. *et al* 2005 *Plasma Phys. Control. Fusion* **47** 545
[16] Satake S. 2006 *et al Plasma and Fusion Res.* **1** 002
[17] Velasco J.L. *et al* 2012 *Plasma Phys. Control. Fusion* **54** 015005
[18] Baldzuhn J. *et al* 1998 *Plasma Phys. Control. Fusion* **40** 967
[19] Murakami S. *et al* 2002 *Nucl. Fusion* **42** L19
[20] Suzuki C. *et al* 2013 *Plasma Phys. Control. Fusion* **55** 014016
[21] Murakami S. *et al* 1995 *Trans. Fusion Technol.* **27** 256
[22] Matsuoka S. *et al* 2011 *Phys. Plasmas* **18** 032511
[23] Sagara A. *et al* 2012 *Fusion Eng. Des.* **87** 594
[24] Wobig H. *et al* 2003 *Nucl. Fusion* **43** 889
[25] Tanaka K. *et al* 2008 *Rev. Sci. Instrum.* **79** 10E702
[26] Wakasa A. *et al* 2010 *Contrib. Plasma Phys.* **50** 582
[27] Dinklage A. *et al* 2007 *Nucl. Fusion* **47** 1265
[28] Tanaka K. *et al* 2010 *Plasma Fus. Res.* **5** S2053
[29] Tanaka K. *et al* 2010 *Fusion Sci. Technol.* **58** 70
[30] Maaßberg H. *et al* 1999 *Plasma Phys. Control. Fusion* **41** 1135